IEEE Access
Multidisciplinary | Rapid Review | Open Access Journal

Received September 9, 2019, accepted September 21, 2019, date of publication September 25, 2019,
date of current version October 23, 2019.

Digital Object Identifier 10.1109/ACCESS.2019.2943622

Mechanism Design and Optimization of a Haptic Master Manipulator for Laparoscopic Surgical Robots

YUNLEI LIANG, LINING SUN, ZHIJIANG DU, ZHIYUAN YAN, AND WEIDONG WANG
State Key Laboratory of Robotics and System, Harbin Institute of Technology, Harbin 150080, China

Corresponding author: Zhiyuan Yan (yanzhiyuan@hit.edu.cn)

This work was supported by the National Key Research and Development Program of China under Grant 2017YFB1304202.

ABSTRACT Serve as the human-robot interface of laparoscopic surgical robot, the master device always plays a crucial role in terms of master-slave manipulation. Growing demands of robot-assisted surgery system also warrant more rational design and optimization for the master manipulator mechanism, which turn out to be important for improving the performance of surgical operations. In this paper, a novel 9 degrees of freedom (DOFs) haptic master manipulator applied to laparoscopic surgical robots is proposed. First of all, the mechanical configuration of the serial master manipulator is presented along with its corresponding kinematic analysis. The proposed strategy can decouple the posture and position completely and to a certain extent simplify the kinematics calculations. Then a mechanism optimization index which synthesizes the global kinematic performances, the global positioning accuracy and the structure length utilization of the manipulator mechanism is introduced. Finally, an improved particle swarm optimization algorithm is proposed to find the optimal mechanism design parameters. The optimization index and algorithm are verified by comparing the optimized parameters with the initial settings. Theoretical analysis and optimization results have demonstrated that the master manipulator can achieve better kinematic performances while maintaining 6 dimensions force feedback.

INDEX TERMS Master manipulator, surgical robots, human-robot interaction, mechanism design, mechanism optimization.

I. INTRODUCTION

Robot-assisted minimal invasive surgery (RMIS), which is famous for its precise position, dexterity enhancement and high success rate in complex surgery, has been greatly developed during the past few years [1]–[4]. The minimally invasive surgical robot can bring the surgeons dexterous instrument control, shorten operation time and reduce the operation risk [5]–[7]. As the human-robot interactive interface of RMIS, the master manipulator is supposed to deliver the surgeon's operations to the slave robot precisely while providing the surgeon with tactile sense properly. Thus, the comfortableness of operation and the success rate of surgery rely heavily on the ergonomics and the capability of master manipulator. Based on the characteristics of RMIS, the master manipulator of laparoscopic surgical robots should have decent kinematic performances, high comfort level of surgical operation, and sufficient ability to implement self-balancing and force feedback. In recent years, many master devices are designed for robot-assisted surgery systems. The most successful minimally invasive surgical robot da Vinci (produced by Intuitive Surgical Inc.) is equipped with a 8 DOFs serial robotic master manipulator [8]–[10], which can be divided into three parts: shoulder, elbow, and wrist. Cable driven mechanism and gear transmission mechanism are both employed in the master manipulator of da Vinci. The joint axes of the wrist part intersect at one point for both simplifying the kinematics analysis process and guaranteeing that the posture of master manipulator can be adjusted flexibly and independently. Because the Touch series (formerly PHANTOM series) have compact structure and small size and can provide precise positioning input and high-fidelity force-feedback output, these haptic devices were employed as the master device of Raven-II, which is a platform for collaborative research on advances in surgical robotics [11], [12]. Touch series are serial-link devices that have 6 DOFs and can

The associate editor coordinating the review of this manuscript and approving it for publication was Jinguo Liu.

feed 3 dimensions force back to operators. The DLR MiroSurge (developed by the German Aerospace Center), which designed to be the expandable and useful system for multiple surgical applications, integrates Omega.7 haptic device as the master manipulator to control the slave surgical robotic arms [13], [14]. Omega.7 (produced by Force Dimension Inc.) can offer 6 DOFs manipulability and an additional grasping DOF. The 3-RUU type parallel mechanism and triaxial concurrent mechanism are used in the Omega.7. The translational and grasping DOFs are actuated and can provide force feedback, whereas the rotatory DOFs are passive and equipped with encoders. The Sigma.7 haptic devices upgraded on the basis of Omega.7 are designed with respect to the requirements in RMIS and other medical applications [15], [16]. The mechanical structure of Sigma.7 is similar to Omeg.7, but all DOFs of Sigma.7 are active. The Senhance surgical system (designed by TransEnterix Inc.) employs haptic handlebars as the master devises. Also, it removes the economic limitations of current robotic systems by using fully reusable instruments [17], [18]. The haptic handlebars characterized by simple structure and small volume are capable of feeding the interaction force between instruments and patients rapidly and precisely. The REVO-I robot-assisted surgery system (produced by meerecompany Inc.) employs serial robotic arms as its master manipulators. It can seamlessly transfer a surgeon's precise hand movement to the robotic arms and make it easier for the surgeon to operate a surgical robotic system [19], [20]. The joint axes of posture adjustment mechanism of REVO-I meet in one point, which is similar to the da Vinci robot. Sang *et al.* [21] developed a novel partly tendon-driven master-slave surgery robot system named MicroHand A to assist minimally invasive surgery. The master manipulator of MicroHand A is a serial robot with 7 DOFs, which can perceive the surgeon's hand motions and provide the operation force feedback. The cable-driven joints are used as positional DOFs and the axes of wrist joints intersect at a common point. Talasaz *et al.* [22] developed a master-slave system to explore the haptic effects in RMIS. The master console includes two haptic wands for transferring the operator's hand motions to the slave manipulators. The dual 5-bar linkage mechanisms which can realize 7 DOFs force reflection are employed in the haptic master devices. It allows for 3 translational DOFs, 3 rotational DOFs, and 1 grasping DOF. Li *et al.* [23] proposed an 8 DOFs haptic manipulator by using the serial-parallel mechanism. The parallel mechanism is designed to control 3 DOFs translational motion and the serial mechanism is a 4 DOFs quadruple-axial concurrent redundant mechanism designed to control three posture angles. Wisanuvej *et al.* [24] presented a joint-space master manipulator for highly articulated robotic instruments in single access surgery. This serial-link manipulator emulates the kinematic structure of highly flexible surgical instruments which is designed to control and use 6 active DOFs to compensate for its own weight and provide force feedback. Takahashi *et al.* [25] developed a master manipulator capable of operating micro neural surgical system. The haptic master manipulator is a serial robotic arm which has 3 translational DOFs and 3 rotational DOFs. The translational part and gripper are actuated by DC motors to realize self-balancing and feed the force information back. Although the master manipulators proposed in the existing studies can be used as the human-robot interaction devices for RMIS, there are still some deficiencies need to be improved. Because the commercial master manipulators such as Omega series and Touch series are not designed for specific surgical robots, these universal haptic devices may not be appropriate for real surgical scenarios. So far, the mechanisms of haptic master manipulator generally fall into three categories: serial mechanisms, parallel mechanisms, and serial-parallel hybrid mechanisms. The parallel mechanisms and the serial-parallel hybrid mechanisms typically possess smaller workspace, complex structure, and less flexibility, which lead to a poor performance of operation in complex surgery. For serial mechanisms, the position and posture of manipulator are not completely decoupled. The pose of manipulator holding point changes with translational motion although the joints of wrist part are fixed. This undesirable coupled motion could cause certain effect on the comfortableness and intuition of operation. In addition, since all the joints of traditional serial manipulators need to be considered in the process of kinematics analysis, the derivation and calculation of the forward and inverse kinematics could be more complex. In order to increase the output torque of active joints, existing haptic devices mainly use gear reducer to produce a large reduction ratio. However, gear transmission mechanism with large reduction ratio will increase the friction moment of active joint, which can influence the compliance and precision of operation. Besides, the designed parameters of traditional mechanism are insufficiently optimized in most cases. Previous researches mainly concentrate on improving the kinematics characteristics of master devices used in laparoscopic surgical robots, but motion precision and structure length capacity factor are not chosen as the optimization index [23], [26], [27]. The optimization schemes dedicated to maximize the kinematic performances of mechanism may generally result in lower motion accuracy and smaller workspace volume. In regard to optimization method, particle swarm optimization algorithm (PSO) has been extensively applied in various parameters optimization process due to its intrinsic advantages such as simple algorithm structure, fast searching speed, and rapid convergence feature. But since the global searching ability of basic PSO is relatively poor and it sometimes end up with premature convergence, appropriate modifications should be made for balancing the local and global searching capabilities of the basic PSO algorithm [28]–[30].

In this paper, a novel 9 DOFs serial master manipulator applied to laparoscopic surgical robot system is presented. The parallelogram mechanism and the active compensation mechanism are both employed to separate the translational motion and rotational motions of the holding point. The transmission scheme that integrates the cable-driven mechanism and the planet-gear speed reducer can further improve the

FIGURE 1. The proposed master manipulator at different viewpoints. (a) Front view. (b) Back view.

compliance of the active joints. The kinematics solutions of the proposed master manipulator are derived and analyzed. A mechanism optimization index which takes the manipulability, kinematic accuracy and structure utilization efficiency of the robotic arm into account is introduced and an improved PSO with penalty term (PTPSO) is proposed to optimize the mechanism design parameters.

This paper is organized as follows. In Section II, the mechanism configuration of the proposed manipulator is introduced. Section III gives the detailed kinematics analysis of the designed master manipulator. In Section IV, an improved PSO method is proposed to find the optimal mechanism structure parameters in terms of a comprehensive optimization index. Discussions and review of the proposed scheme can be found in Section V. Finally, in Section VI, the conclusion is drawn.

II. DESIGN CONCEPT AND STRUCTURE

During the process of RMIS, the slave robot typically repeats the motions of master manipulator operated by the surgeon directly. In order to meet the requirements of minimally invasive surgery, the master manipulator is supposed to possess qualities such as large workspace, decent manipulability, and the ability to achieve 3 DOFs translational motions, 3 DOFs rotational motions, and 1 DOF grasping motion. Considering the performance demands of surgical master devices, a 9 DOFs serial manipulator is designed in this paper as shown in Fig. 1. In this section, the coupling relationship between the position and posture of traditional master manipulators is analyzed. Besides, the mechanical structure and transmission scheme of the proposed haptic device are introduced.

A. COUPLED MOTION ANALYSIS FOR THE SERIAL MASTER MANIPULATOR

In general, it is the inherent characteristics of the serial robotic arm that lead to the coupled relation between the position and posture of the endpoint of manipulator. Some existing surgical master manipulators employ multiaxial concurrent wrist mechanism to simplify the kinematics analysis. Fig. 2 shows

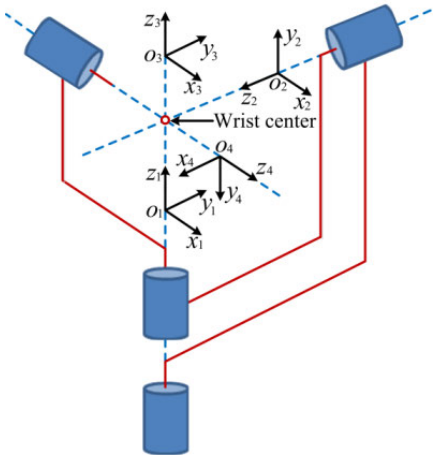

FIGURE 2. Kinematic model of the wrist part.

the kinematic model of the wrist part. It can be seen from Fig. 2 that the links of wrist rotate around the intersection point of joint axes, so the position of the holding point will not be affected by the rotational motions of the wrist part. That is, the adjustment of posture does not change the position of manipulator's holding point. However, though providing no other rotational motion of the manipulator's wrist, the posture of the holding point still can change in the course of position adjustment. Fig. 3 shows the changing situation of the posture of finger griper when the manipulator locates at different positions. It can be seen from Fig. 3, for traditional master manipulators, the position changes of holding point will influence its posture. The posture of manipulator's gripper is depended on two factors: the rotation angles of wrist joints and the position of holding point. The coupled relationship between the position and posture of manipulator results in an undesirable posture change of the gripper, so that it is difficult for a surgeon to control the posture of the grippers precisely during an operation. Considering the surgical application scenarios of the master manipulators, coupled motion indeed

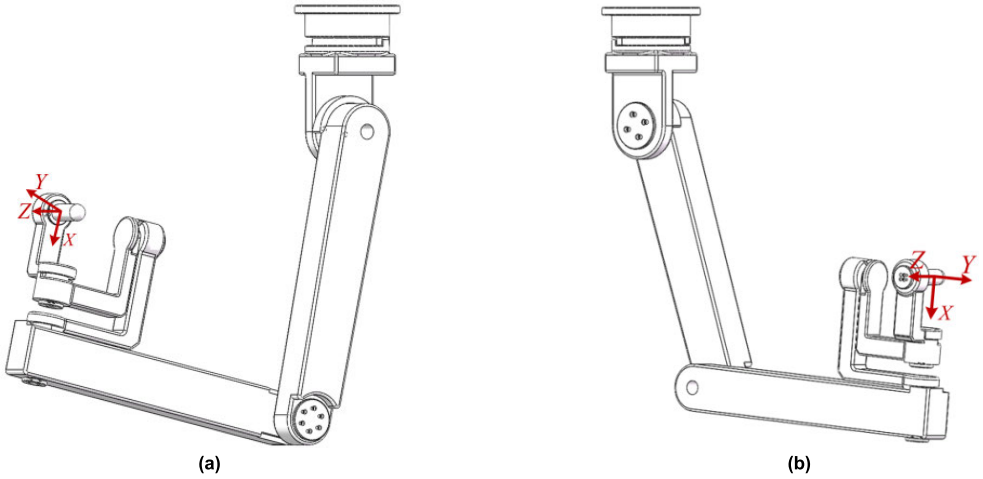

FIGURE 3. The posture of finger gripers when the manipulator locates at different positions. (a) At position 1. (b) At position 2.

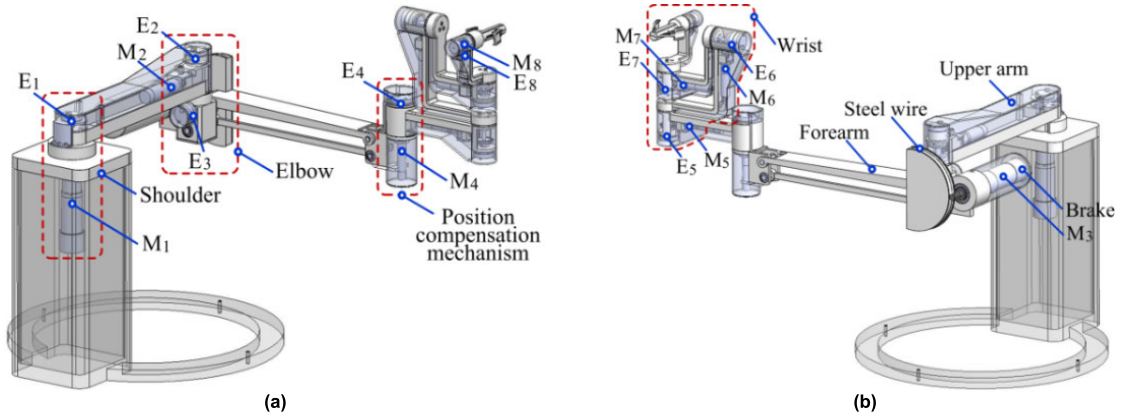

FIGURE 4. The basic structure of the designed 9 DOFs manipulator. (a) Front view. (b) Back view.

impacts the comfortableness and intuition of the surgeon. In order to solve this problem, the master manipulator needs to be designed rationally to separate the position adjustment mechanism and the posture adjustment mechanism.

B. MECHANICAL DESIGN OF THE MASTER MANIPULATOR

Based on the application scenarios and the performance requirements of master manipulator used in laparoscopic surgical robots, the mechanical structure of the proposed manipulator needs to meet the following requirements.

(1) The manipulator should have good manipulability and its workspace shall be large enough.

(2) The manipulator should be able to adjust its position and posture actively while providing necessary force feedback.

(3) The position and posture of the holding point should be mutually independent.

(4) The friction moment of the joints should be low enough.

Based on the above requirements, we designed a novel 9 DOFs serial manipulator which is composed of the position adjusting mechanism and the posture adjusting mechanism. Fig. 4 shows the basic structure of the designed 9 DOFs manipulator. In Fig. 4, $E_1, E_2, \cdots, E_8$ and $M_1, M_2, \cdots, M_8$ denote the absolute encoders and the motors of 8 active joints, respectively. From Fig. 4, we can know that the proposed manipulator is composed of shoulder, upper arm, elbow, forearm, position compensation mechanism, and wrist. For ensuring both the flexibility and comfortableness of operation, the active joints need to output certain torques to balance the gravitational torque, friction torque, inertial torque, centrifugal torque, and Coriolis torque of mechanism. Among these torques, the value of gravitational torque is much greater than others. As shown in Fig. 4, the driving torque of elbow pitch joint needs to be large enough to balance the gravity of forearm, position compensation mechanism, and wrist. In this paper, the transmission system of elbow pitch joint synthesizes steel wire and gear reducer to get a large reduction ratio and increase the output torque, which could avoid increasing the volume and friction torque of transmission mechanism. The brake is installed on the shaft of Motor 3 to ensure the master manipulator would not fall from a height so that damage the mechanism when the power is failure. Fig. 5

TABLE 1. D-H parameters for each joint of the master manipulator.

$Joint_i$	α_{i-1} (rad)	a_{i-1} (mm)	d_i (mm)	θ_i (rad)	Motion range (°)
1	0	0	0	q_1	[-50, 40]
2	0	a_1	$-d_2$	q_2-π/2	[-60, 60]
3	-π/2	0	d_3	q_3	[-70, 70]
4	0	a_3	0	q_4	[-70, 70]
5	π/2	a_4	d_5	q_5	[-100, 110]
6	0	a_5	d_6	q_6-π/2	[-120, 120]
7	-π/2	0	0	q_7	[-130, 160]
8	π/2	0	0	q_8+π/2	[-45, 45]
9	π/2	0	0	q_9-π/2	unlimited

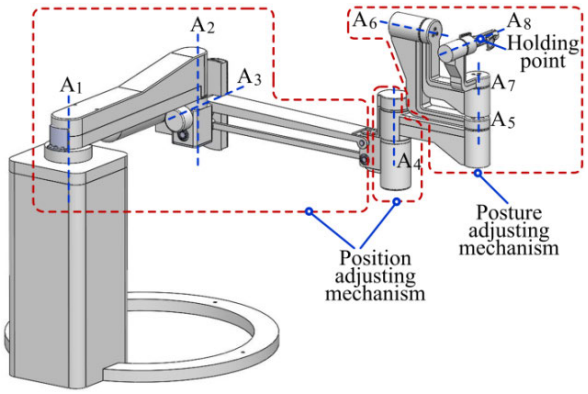

FIGURE 5. The three-dimensional model of the proposed manipulator.

shows the three dimensional model of the proposed manipulator. In Fig. 5, $A_1, A_2, \cdots, A_8$ represent the corresponding rotation axes of active joints, respectively. Also, from Fig. 5, we can know that the position adjusting mechanism has 4 rotational DOFs and the posture adjusting mechanism has 4 rotational DOFs and 1 grasping DOF. The rotation angle of joint 7 needs to be less than 90° to avoid the manipulator reaching the singular configuration when A_6 is coincident with A_8 and joint 5 can extend the motion range of joint 7 by rotating redundantly. Among the 9 DOFs of the designed manipulator, 8 rotational DOFs are active. The position and posture of the holding point can be adjusted respectively by the position and posture adjusting mechanism within the workspace. In order to eliminate the coupling relationship between the position and posture of the holding point, parallelogram mechanism and position compensating mechanism are used in the designed manipulator. Fig. 6 and Fig. 7 show the decoupling principles of the parallelogram mechanism and the position compensating mechanism, respectively.

We can see that from Fig. 6, because of the structure constraint of parallelogram mechanism, link cd is always parallel to link ab during the movement of the manipulator. The mechanism can ensure that the axis A_4 is always parallel to A_1. In Fig. 7, ZP1, ZP2, and ZP4 respectively denote the zero references of A_1, A_2, and A_4. q_1 and q_2 respectively denotes the rotational angles of A_1 and A_2. As shown in Fig. 7, the rotation angle of the position compensating mechanism is equal to the sum of yaw angles of the shoulder and elbow part in the opposite direction. In this way, the yaw angle of the position compensating mechanism relative to the base coordinate system will always stay fixed regardless of the motion of manipulator. Under the constraints of the parallelogram mechanism and the position compensating mechanism, the posture of wrist turns out to be independent to the position adjusting mechanism. That is, the position and posture of holding point are completely decoupled.

III. KINEMATICS ANALYSIS

In the process of RMIS, surgeon controls the slave surgical robots by operating the grippers of the master manipulator. Essentially, the master device transmits the hand motions of surgeon to the slave robots through its position and posture. In order to obtain the position and posture of the grasper, the forward kinematics solution of the master manipulator should be derived. During the course of rebuilding the master-slave mapping, the master manipulator should actively adjust its position and posture according to the position and posture of the instrument distal end, which needs to solve the inverse kinematics equations of the proposed manipulator. In addition, the kinematics equations relating joint angles to Cartesian variables are needed for operating a haptic device and optimizing the mechanical structure parameters.

A. FORWARD KINEMATICS ANALYSIS

In this paper, the direct kinematics equations of the proposed serial manipulator are derived by applying the Denavit-Hartenberg (D-H) method. The established D-H coordinate system based on the mechanical structure of the haptic device is shown in Fig. 8. The coordinate axis Z_i coincides with the rotation axis of the i-th joint. For describing the motion characteristics of the parallelogram mechanism, a virtual rotation axis and its corresponding coordinate system $\{X_4, Y_4, Z_4\}$ are established. The D-H method uses four parameters $(\alpha_{i-1}, a_{i-1}, \theta_i, d_i)$ to describe the geometrical relationship between the $(i-1)$-th link and the i-th link. Table 1 shows the D-H parameters of each joint shown in Fig. 8. Where q_i represents the rotation angle relative to original position of the i-th link.

After the D-H parameters are determined, the homogenous transformation matrix of rotary and translation joint relating

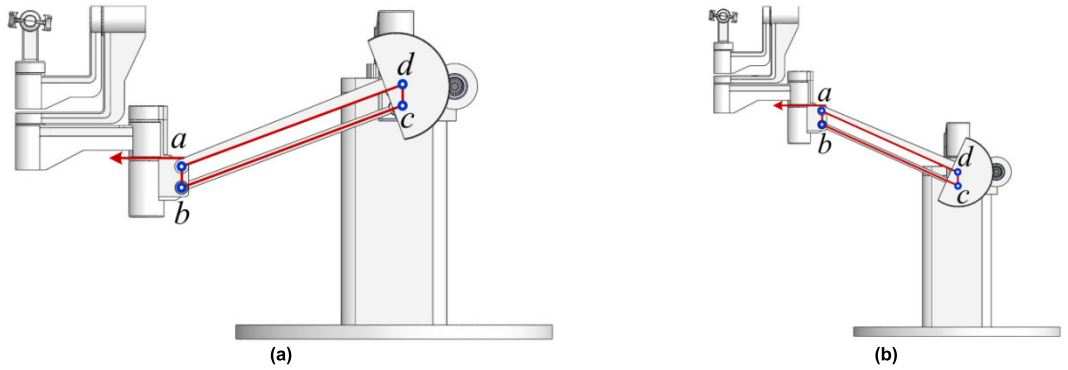

FIGURE 6. The movement characteristics of the parallelogram mechanism. (a) Pitch down. (b) Pitch up.

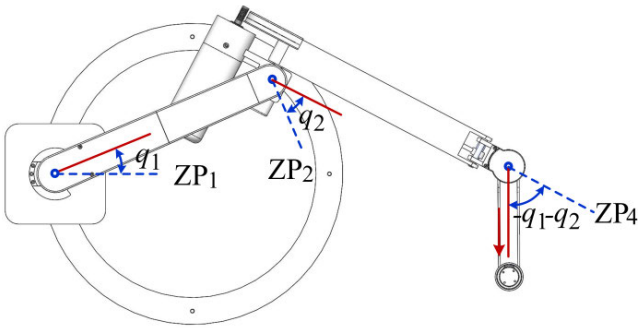

FIGURE 7. The decoupling principles of the position compensating mechanism.

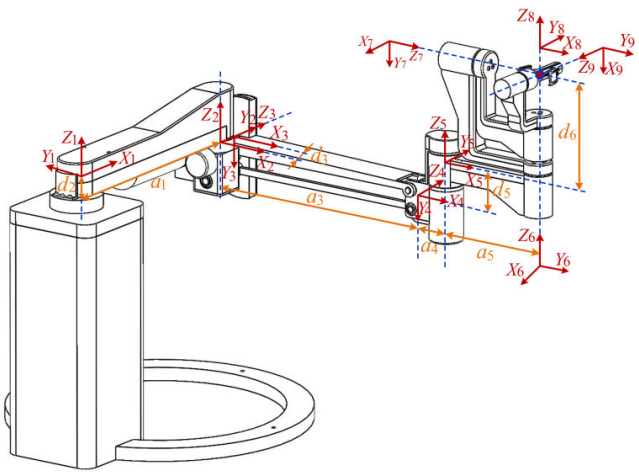

FIGURE 8. Kinematic model of the proposed master manipulator.

the $(i-1)$-th link to the i-th link can be defined as follows:

$$
{}^{i-1}_{i}T = \begin{bmatrix} c\theta_i & -s\theta_i & 0 & a_{i-1} \\ s\theta_i c\alpha_{i-1} & c\theta_i c\alpha_{i-1} & -s\alpha_{i-1} & -s\alpha_{i-1} d_i \\ s\theta_i s\alpha_{i-1} & c\theta_i s\alpha_{i-1} & c\alpha_{i-1} & c\alpha_{i-1} d_i \\ 0 & 0 & 0 & 1 \end{bmatrix} \tag{1}
$$

According to the geometric constraint of parallelogram mechanism and the operating principle of the active compensation mechanism, we can know that $q_4 = -q_3$ and $q_5 = -q_1 - q_2$.The transformation matrix from base coordinate frame to tool coordinate frame is solved as follows:

$$
\begin{aligned}
{}^{0}_{n}T &= {}^{0}_{1}T \times {}^{1}_{2}T \cdots \times {}^{n-1}_{n}T \\
&= \begin{bmatrix} R & P \\ 0 & 1 \end{bmatrix} = \begin{bmatrix} n_x & o_x & a_x & p_x \\ n_y & o_y & a_y & p_y \\ n_z & o_z & a_z & p_z \\ 0 & 0 & 0 & 1 \end{bmatrix},
\end{aligned} \tag{2}
$$

where R is the 3×3 rotation matrix and P is the 3×1 position vector. Synthesize (1), (2), and the D-H parameters listed in Table 1, the position and posture of the holding point can be formulated as follows:

$$
R = \begin{bmatrix} R_{11} & R_{12} & R_{13} \\ R_{21} & R_{22} & R_{23} \\ R_{31} & R_{32} & R_{33} \end{bmatrix},
$$

$$
\begin{cases}
R_{11} = cq_6cq_9sq_7 + cq_8sq_6sq_9 + cq_6cq_7sq_8sq_9 \\
R_{12} = cq_8cq_9sq_6 - cq_6sq_7sq_9 + cq_6cq_7cq_9sq_8 \\
R_{13} = sq_6sq_8 - cq_6cq_7cq_8 \\
R_{21} = cq_9sq_6sq_7 - cq_6cq_8sq_9 + cq_7sq_6sq_8sq_9 \\
R_{22} = cq_7cq_9sq_6sq_8 - cq_6cq_8cq_9 - sq_6sq_7sq_9 \\
R_{23} = -cq_6sq_8 - cq_7cq_8sq_6 \\
R_{31} = sq_7sq_8sq_9 - cq_7cq_9 \\
R_{32} = cq_7sq_9 + cq_9sq_7sq_8 \\
R_{33} = -cq_8sq_7,
\end{cases} \tag{3}
$$

$$
P = \begin{bmatrix} a_1cq_1 + d_3c(q_1+q_2) + a_4s(q_1+q_2) \\ +a_3cq_3s(q_1+q_2) \\ a_1sq_1 - a_5 + d_3s(q_1+q_2) - a_3cq_3c(q_1+q_2) \\ -a_4c(q_1+q_2) \\ d_6 - d_2 + d_5 - a_3sq_3 \end{bmatrix}, \tag{4}
$$

where sq_i and cq_i are the abbreviation of $\sin(q_i)$ and $\cos(q_i)$, respectively. We can draw two conclusions from (3) and (4): first, the rotation matrix of the designed manipulator is only determined by the rotation angles of wrist part (q_6, q_7, q_8, and q_9). Second, the position vector of the designed manipulator is only determined by linkage dimensions (a_1, a_3, a_4, a_5, d_2, d_3, d_5, and d_6) and the rotation angles of shoulder and elbow parts (q_1, q_2, and q_3). That is, the position and

orientation of the holding point are decoupled completely and can be adjusted respectively by the position and posture adjusting mechanisms. In contrast with the proposed strategy, the pose of traditional serial master robots depends on all joint angles, which will greatly increase the complexities of analysis and computation. In addition, the master manipulator possesses mutually independent position and orientation adjusting mechanism can provide more comfortable and intuitive operating feeling.

B. INVERSE KINEMATICS ANALYSIS

In the active motion process of master manipulator, the inverse kinematics analysis is used to find the rotation angle of each joint given the position and orientation of the holding point relative to the base frame and the values of all of the geometric link parameters. Suppose the transformation matrix from base coordinate frame to tool coordinate frame is known and can be given as follows:

$$ {}^{0}_{n}T = \begin{bmatrix} n_x & o_x & a_x & p_x \\ n_y & o_y & a_y & p_y \\ n_z & o_z & a_z & p_z \\ 0 & 0 & 0 & 1 \end{bmatrix} \tag{5} $$

Since the position and posture of the designed manipulator are mutually independent, the position vector P and the rotation matrix R can be used to solve the joint angles of position adjustment mechanism (q_1, q_2, and q_3) and posture adjusting mechanism (q_6, q_7, q_8, and q_9), respectively. After combining (4) and (5), 3 equalities can be obtained to solve 3 unknown parameters (q_1, q_2, and q_3).

$$ \begin{aligned} p_x - a_1cq_1 &= d_3c(q_1+q_2) + a_4s(q_1+q_2) \\ &\quad + a_3cq_3s(q_1+q_2) \qquad (6) \\ p_y - a_1sq_1 + a_5 &= d_3s(q_1+q_2) - a_3cq_3c(q_1+q_2) \\ &\quad - a_4c(q_1+q_2) \qquad (7) \\ p_z &= d_6 - d_2 + d_5 - a_3sq_3 \qquad (8) \end{aligned} $$

According to (8), q_3 can be solved as:

$$ q_3 = \arcsin\left(\frac{d_6 - d_2 + d_5 - p_z}{a_3}\right), \quad q_3 \in [q_{3min}, q_{3max}], \tag{9} $$

where q_{imin} and q_{imax} are the minimum and maximum value of q_i, respectively. Squaring both sides of (6) and (7), then add the results together, we get.

$$ \begin{aligned} cq_1 &= a - bsq_1, \\ a &= p_x^2 + a_1^2 + (p_y + a_5)^2 - d_3^2 - (a_3cq_3 + a_4)^2/2p_xa_1, \\ b &= \frac{p_y + a_5}{p_x} \end{aligned} \tag{10} $$

According to (10) and the properties of trigonometric function, the equation for q_1 can be derived as:

$$ (a - bsq_1)^2 + s^2q_1 = 1 \tag{11} $$

Then the value of q_1 can be given by (12) and (13).

$$ sq_1 = \frac{2ab \pm \sqrt{4a^2b^2 - 4(b^2+1)(a^2-1)}}{2(b^2+1)}, \quad sq_1 \in [sq_{1min}, sq_{1max}] \tag{12} $$

$$ (a - bsq_1)^2 + s^2q_1 = 1 \tag{13} $$

Combining (6), (7), and deriving the expressions $s(q_1+q_2)$ and $c(q_1+q_2)$, we can get (14).

$$ \begin{aligned} &\tan(q_1+q_2) \\ &= \frac{s(q_1+q_2)}{c(q_1+q_2)} \\ &= \frac{(a_3cq_3+a_4)(p_x - a_1cq_1) + d_3(p_y + a_5 - a_1sq_1)}{d_3(p_x - a_1cq_1) - (a_3cq_3+a_4)(p_y + a_5 - a_1sq_1)} \end{aligned} \tag{14} $$

Then q_2 can be derived as follows:

$$ q_2 = \arctan\left[\frac{(a_3cq_3+a_4)(p_x - a_1cq_1) + d_3(p_y + a_5 - a_1sq_1)}{d_3(p_x - a_1cq_1) - (a_3cq_3+a_4)(p_y + a_5 - a_1sq_1)}\right] - q_1, \quad q_2 \in [q_{2min}, q_{2max}] \tag{15} $$

At this point, the joint angles of the position adjusting mechanism are obtained. Based on the analysis above, the orientation of the designed manipulator has no connection with the shoulder and elbow parts. So, the posture of the holding point can also be expressed as:

$$ R = {}^{0}_{6}R^{6}_{7}R^{7}_{8}R^{8}_{9}R = \begin{bmatrix} n_x & o_x & a_x \\ n_y & o_y & a_y \\ n_z & o_z & a_z \end{bmatrix} \tag{16} $$

Multiplying both sides of (16) by $({}^{6}_{7}R)^{-1} \times ({}^{0}_{6}R)^{-1}$, we can obtain (17).

$$ ({}^{6}_{7}R)^{-1}({}^{0}_{6}R)^{-1}R = {}^{7}_{8}R^{8}_{9}R \tag{17} $$

Expanding both sides of (17), we can obtain.

$$ \begin{aligned} n_zsq_7 + n_xcq_6cq_7 + n_ycq_7sq_6 &= sq_8sq_9 \\ o_zsq_7 + o_xcq_6cq_7 + o_ycq_7sq_6 &= cq_9sq_8 \\ -a_zsq_7 - a_xcq_6cq_7 - a_ycq_7sq_6 &= cq_8 \\ n_xcq_6sq_7 - n_zcq_7 + n_ysq_6sq_7 &= cq_9 \\ -o_xcq_6sq_7 + o_zcq_7 - o_ysq_6sq_7 &= sq_9 \\ a_xcq_6sq_7 - a_zcq_7 + a_ysq_6sq_7 &= 0 \\ n_xsq_6 - n_ycq_6 &= cq_8sq_9 \\ o_xsq_6 - o_ycq_6 &= cq_8cq_9 \\ a_xsq_6 - a_ycq_6 &= sq_8 \end{aligned} \tag{18} $$

According to (18) and the properties of trigonometric function, the following equation can be formulated as:

$$ (sq_8sq_9)sq_9 + (cq_9sq_8)cq_9 = sq_8 \tag{19} $$

According to (18) and (19), the following equation can be formulated as:

$$ n_xo_zcq_6 - n_zo_xcq_6 + n_yo_zsq_6 - n_zo_ysq_6 = a_xsq_6 - a_ycq_6 \tag{20} $$

Then q_6 can be derived as follows:

$$q_6 = \arctan(\frac{n_x o_z - n_z o_x + a_y}{a_x + n_z o_y - n_y o_z}), \quad q_6 \in [q_{6min}, q_{6max}] \tag{21}$$

Multiplying both sides of (16) by $({}^0_6R)^{-1}$, we can obtain (22).

$$({}^0_6R)^{-1}R = {}^6_7R^7_8R^8_9R \tag{22}$$

Expanding both sides of (22), we can obtain (23).

$$\begin{aligned}
&({}^0_6R)^{-1}R \\
&= \begin{bmatrix} -n_x cq_6 - n_y sq_6 & -o_x cq_6 - o_y sq_6 & -a_x cq_6 - a_y sq_6 \\ n_x sq_6 - n_y cq_6 & o_x sq_6 - o_y cq_6 & a_x sq_6 - a_y cq_6 \\ n_z & o_z & a_z \end{bmatrix} \\
&= {}^6_7R^7_8R^8_9R \\
&= \begin{bmatrix} -cq_9 sq_7 - cq_7 sq_8 sq_9 & sq_7 sq_9 - cq_7 cq_9 sq_8 & cq_7 cq_8 \\ cq_8 sq_9 & cq_8 cq_9 & sq_8 \\ sq_7 sq_8 sq_9 - cq_7 cq_9 & cq_7 sq_9 + cq_9 sq_7 sq_8 & -cq_8 sq_7 \end{bmatrix}
\end{aligned} \tag{23}$$

According to (23), the following equation can be formulated as:

$$\begin{aligned}
\tan(q_7) &= -\frac{({}^6_7R^7_8R^8_9R)(3,3)}{({}^6_7R^7_8R^8_9R)(1,3)}, \\
\tan(q_8) &= cq_7\frac{({}^6_7R^7_8R^8_9R)(2,3)}{({}^6_7R^7_8R^8_9R)(1,3)}, \\
\tan(q_9) &= \frac{({}^6_7R^7_8R^8_9R)(2,1)}{({}^6_7R^7_8R^8_9R)(2,2)}
\end{aligned} \tag{24}$$

Then q_7, q_8, and q_9 can be derived as follows:

$$\begin{aligned}
q_7 &= \arctan(\frac{a_z}{a_x cq_6 + a_y sq_6}), \quad q_7 \in [q_{7min}, q_{7max}], \\
q_8 &= \arctan(\frac{a_x sq_6 cq_7 - a_y cq_6 cq_7}{-a_x cq_6 - a_y sq_6}), \quad q_8 \in [q_{8min}, q_{8max}], \\
q_9 &= \arctan(\frac{n_x sq_6 - n_y cq_6}{o_x sq_6 - o_y cq_6}), \quad q_9 \in [q_{9min}, q_{9max}]
\end{aligned} \tag{25}$$

So far, all the joint angles of the designed master manipulator are obtained. Based on the analysis above, we can know that the proposed strategy can simplify calculation and analysis process of inverse kinematics.

C. JACOBIAN ANALYSIS

Jacobian matrix is one of the important parameters of robots, which can describe the relationship between the velocity in Cartesian space and the velocity in joint space. Differentiation with respect to time of the results of forward kinematics analysis yields a set of equations of the form.

$$\begin{pmatrix} v_{3\times1} \\ w_{3\times1} \end{pmatrix} = J(q)\dot{q}, \tag{26}$$

where $v_{3\times1}$ and $w_{3\times1}$ are the linear velocity vector and angular velocity vector in Cartesian space, respectively; $\dot{q}$ is an n dimensional vector composed of the joint rates; $J(q)$ is a $6 \times n$ matrix which called the Jacobian matrix. The differential transform method is used to solve the closed-form expression of the Jacobian matrix. Suppose $\vec{n} = [n_x, n_y, n_z]$, $\vec{o} = [o_x, o_y, o_z]$, $\vec{a} = [a_x, a_y, a_z]$, and $\vec{p} = [p_x, p_y, p_z]$ are 4 column vectors of ${}^n_iT$, which is the transformation matrix from the i-th coordinate frame to tool coordinate frame. Then the i-th column vector of the Jacobian matrix relative to the tool frame can be derived as:

$${}^T J_i(q) = \begin{bmatrix} -n_x p_y + n_y p_x \\ -o_x p_y + o_y p_x \\ -a_x p_y + a_y p_x \\ n_z \\ o_z \\ a_z \end{bmatrix} \tag{27}$$

Based on the transformation relation between the base frame and the tool frame, the Jacobian matrix relative to the base frame can be derived as:

$${}^B J(q) = \begin{bmatrix} R & 0_{3\times3} \\ 0_{3\times3} & R \end{bmatrix} {}^T J_i(q) \tag{28}$$

According to (26), (28), and the designed mechanism of the master manipulator, the velocity of the holding point relative to the base coordinate frame can be expressed as follows:

$$\begin{pmatrix} v_{3\times1} \\ w_{3\times1} \end{pmatrix} = {}^B J(q) \cdot [\dot{q}_1, \dot{q}_2, \dot{q}_3, \dot{q}_4, \dot{q}_5, \dot{q}_6, \dot{q}_7, \dot{q}_8, \dot{q}_9]^T \tag{29}$$

However, the joint angles q_4 and q_5 are the auxiliary variables, which cannot reflect the motion of the proposed manipulator. Based on the characteristics of the designed mechanism, we can know that $q_4 = -q_3$ and $q_5 = -q_1 - q_2$, that is, $\dot{q}_4 = -\dot{q}_3$ and $\dot{q}_5 = -\dot{q}_1 - \dot{q}_2$. So, the Jacobian matrix relative to the base frame can be modified and (29) can be changed into the following expression.

$$\begin{pmatrix} v_{3\times1} \\ w_{3\times1} \end{pmatrix} = J(q) \cdot [\dot{q}_1, \dot{q}_2, \dot{q}_3, \dot{q}_6, \dot{q}_7, \dot{q}_8, \dot{q}_9]^T, \tag{30}$$

where $J(q)$ is 6×7 matrix which denotes the modified Jacobian matrix relative to the base frame. According to the above analysis, the following equation can be obtained.

$$\begin{aligned}
J(q) = \big[&{}^B J_1(q) - {}^B J_5(q), {}^B J_2(q) - {}^B J_5(q), {}^B J_3(q) - {}^B J_4(q), \\
&{}^B J_6(q), {}^B J_7(q), {}^B J_8(q), {}^B J_9(q)\big]
\end{aligned} \tag{31}$$

Combining (27), (28), and (31), the expression of $J(q)$ can be formulated as:

$$J(q) = \begin{bmatrix} J_v & 0_{3\times4} \\ 0_{3\times3} & J_w \end{bmatrix} \tag{32}$$

$$J_w = \begin{bmatrix} 0 & sq_6 & -cq_6 sq_7 & sq_6 sq_8 - cq_6 cq_7 cq_8 \\ 0 & -cq_6 & -sq_6 sq_7 & -cq_6 sq_8 - cq_7 cq_8 sq_6 \\ 1 & 0 & cq_7 & -cq_8 sq_7 \end{bmatrix} \tag{33}$$

$$J_v = \begin{bmatrix} J_{11} & J_{12} & J_{13} \\ J_{21} & J_{22} & J_{23} \\ J_{31} & J_{32} & J_{33} \end{bmatrix},$$

$$\begin{cases} J_{11} = a_3 c q_3 c(q_1+q_2) + a_4 c(q_1+q_2) \\ \qquad - d_3 s(q_1+q_2) - a_1 s q_1 \\ J_{12} = a_3 c q_3 c(q_1+q_2) + a_4 c(q_1 \\ \qquad + q_2) - d_3 s(q_1+q_2) \\ J_{13} = -a_3 s(q_1+q_2) s(q_3) \\ J_{21} = a_3 c q_3 s(q_1+q_2) + a_4 s(q_1+q_2) \\ \qquad + d_3 c(q_1+q_2) + a_1 c q_1 \\ J_{22} = a_3 c q_3 s(q_1+q_2) + a_4 s(q_1 \\ \qquad + q_2) + d_3 c(q_1+q_2) \\ J_{23} = a_3 c(q_1+q_2) s(q_3) \\ J_{31} = 0 \\ J_{32} = 0 \\ J_{33} = -a_3 c(q_3), \end{cases} \tag{34}$$

From (32), (33), and (34), we can know that the linear velocity vector only depends on the position adjusting mechanism and the angular velocity vector only depends on the posture adjusting mechanism, which is consistent with the design goal.

IV. OPTIMIZATION OF DESIGN PARAMETERS

One of the important issues for designing the master manipulator used in surgical robots is optimizing the design parameters which will influence the operation performance. The transmission scheme and DOFs configuration of the proposed manipulator are determined by the application to be carried out and the optimized object of the designed haptic device is the link length. In this section, kinematic performances, positioning accuracy, and structure length utilization ratio are considered comprehensively in the proposed optimization index. A modified PSO with a penalty term (PTPSO) is designed to find the appropriate link lengths of the master manipulator. The optimized results are compared with the arbitrary design parameters to verify optimization effects.

A. OPTIMIZATION INDEX DESIGN

As is known, dexterity is one of the key performance indices for surgical haptic device. The performance index able to measure the dexterity can be defined as follows:

$$k = \frac{\sigma_{max}(J)}{\sigma_{min}(J)}, \tag{35}$$

where k is the condition number of the Jacobian matrix; $\sigma_{max}(J)$ and $\sigma_{\min}(J)$ are the maximum singular value and minimum singular value of the Jacobian matrix, respectively. The analytic expression of k is derived in the Appendix. Since k is a local performance index which can only reflect the isotropic of motion transmission at a certain location, a strategy able to measure the dexterity throughout the entire workspace would be preferable. The global conditioning index (GCI) is meant to assess the distribution of the aforementioned condition number over the whole workspace [31]. The GCI defined as (36) gives the overall situation of dexterity and can be used as global performance evaluation index for the master manipulator.

$$GCI = \frac{\int_W \frac{1}{k} dW}{\int_W dW}, \tag{36}$$

where W is a workspace defined in the Cartesian coordinate system. The smaller the k is, the smaller error magnification of the motion transmission due to the kinematic and static transformations between the joint and Cartesian spaces is. That is, the value of GCI should be positively correlated with the kinematic performances of mechanism. However, GCI is the average of global performance which cannot reflect the fluctuation situation of dexterity over the workspace [23]. When the variance of operating performance index is large, there will be some areas of the workspace with poor dexterity. So, the global conditioning mean square error index (GCSEI) defined as (37) is also introduced as the evaluation criteria for avoiding the performance deficiencies.

$$GCSEI = \sqrt{\frac{\int_W (\frac{1}{k} - GCI)^2 dW}{\int_W dW}}, \tag{37}$$

GCSEI assesses the rangeability of motion transmission performance over the workspace by means of variance analysis method. The smaller the GCSEI is, the more consistent the dexterity performance is. In order to comprehensively evaluate the kinematic performances of mechanism, the optimization index should include both GCI and GCSEI. In this paper, the fitness function for evaluating the kinematic performances of mechanism can be expressed as follows:

$$f_k = GCSEI - GCI = \sqrt{\frac{\int_W (\frac{1}{k} - \frac{\int_W \frac{1}{k} dW}{\int_W dW})^2 dW}{\int_W dW}} - \frac{\int_W \frac{1}{k} dW}{\int_W dW}, \tag{38}$$

where f_k is the fitness function for the kinematic performances of haptic device. Based on the above analysis, the smaller the f_k is, the better overall performance of the mechanism we can get. The motor and planet gear speed reducer are integrated in each rotating joint to improve the output torque. However, the planet gear speed reducer has a larger backlash, which will increase the nonlinearity of motion, and then increase the positioning error. Since the master manipulator needs to actively adjust its position and posture during the operation for rebuilding the master-slave mapping and homing, the movement accuracy of the holding point in Cartesian space can have significant effects on the quality and precision of RMIS. The effects of backlash on positioning accuracy can be obtained based on the link lengths, backlash size and forward kinematics. For comprehensively evaluating the positioning performance of the master manipulator in global scope, the global precision index (GPI) is employed in this

paper. In order to describe the motion precision quantitatively, the minimum positioning error of holding point at a certain location can be defined as follows:

$$e_{max} = \max(\sqrt{(x_p - x_e)^2 + (y_p - y_e)^2 + (z_p - z_e)^2}), \quad (39)$$

where e_{max} is the defined minimum positioning error; (x_e, y_e, z_e) represents the expected position coordinates of holding point and (x_p, y_p, z_p) represents the possible position coordinates of holding point under the influence of backlash. The definition of GPI is similar to GCI and can be expressed as follows:

$$GPI = \frac{\int\limits_W e_{max} dW}{\int\limits_W dW} \quad (40)$$

GPI is analyzed for assessing the positioning performance of the designed manipulator. The fitness function for the kinematic accuracy of mechanism is defined as follows:

$$f_p = GPI = \frac{\int\limits_W e_{max} dW}{\int\limits_W dW}, \quad (41)$$

where f_p is the fitness function for the motion precision of the proposed manipulator. By reducing f_p we can improve the localization accuracy of the designed master manipulator. For a master device of the robot-assisted surgery system, its reachable workspace volume should be maximal. However, if the workspace volume is used as optimization criterion directly, the optimization result will maximize the link lengths of mechanism. Therefore, both the reachable workspace volume and the dimensions of links should be considered as the components of the optimization index. The structure length utilization factor defined as (42) is the ratio of the cube root of the reachable workspace volume to the link length sum of the robot manipulator.

$$f_l = \frac{L}{\sqrt[3]{V}}, \quad (42)$$

where f_l is the fitness function for the structure length utilization factor of mechanism; V is the workspace volume of the proposed manipulator; L is the sum of link lengths of mechanism. A smaller value of f_l indicates a better utilization of structure length. So far, we have introduced all the concerned factors and the corresponding evaluation indexes we want to consider in designing the optimization method. And because of the special application scenarios of RMIS, the kinematic characteristics and the volume of reachable workspace turn out to be more important for the proposed manipulator. Therefore, when considering the overall optimization function, the weights of f_k, f_p, and f_l are chosen to be 4, 2, and 1, respectively. As such, the overall fitness function that takes f_k, f_p, and f_l into account can be formulated as follows:

$$f = 4\frac{f_k - f_{kmin}}{f_{kmax} - f_{kmin}} + 2\frac{f_l - f_{lmin}}{f_{lmax} - f_{lmin}} + \frac{f_p - f_{pmin}}{f_{pmax} - f_{pmin}}, \quad (43)$$

where f is the overall fitness function of mechanism optimization; f_{kmin}, f_{pmin}, and f_{lmin} are the minimum values of f_k, f_p, and f_l, respectively; f_{kmax}, f_{pmax}, and f_{lmax} are the maximum values of f_k, f_p, and f_l, respectively.

B. IMPROVED PARTICLE SWARM OPTIMIZATION ALGORITHM DESIGN

After the overall fitness function f is determined, a global PSO algorithm that takes f as the optimization goal is designed in search of the appropriate link lengths. Although the basic PSO has been widely used for searching the optimal parameters, its capability in global searching still needs to be improved for avoiding premature convergence. Existing researches mainly improve the searching performance of the basic PSO by using constriction factor [32], time varying nonlinear inertia weight [33], time varying linear inertia weight [34], [35], dynamic adaptation [36], and random inertia weight [37]. We can assume that the number of particles is M, the number of iterations is T and the dimensionality of search space is D in the basic PSO model. Then the d-th dimensional position and velocity of the i-th particle in the t-th iteration can be respectively defined as x_{id}^t and v_{id}^t. Where $i = 1, 2, 3, \cdots, M$, $t = 1, 2, 3, \cdots, T$, and $d = 1, 2, 3, \cdots, D$. $v_{id}^t \in [-v_{max}, v_{max}]$, where v_{max} is a problem-dependent constant defined in order to clamp the excessive roaming of particles. The velocity and position updating rule of each particle can be given by:

$$v_{id}^{t+1} = w \times v_{id}^t + c_1 r_1 \left(p_{id}^t - x_{id}^t\right) + c_2 r_2 \left(g_d^t - x_{id}^t\right), \quad (44)$$

$$x_{id}^{t+1} = x_{id}^t + v_{id}^{t+1}, \quad (45)$$

where $w \geqslant 0$ is defined as the inertia weight factor; c_1 and c_2 are the acceleration coefficients; r_1 and r_2 are two independent random numbers uniformly distributed in the range of [0, 1]; p_{id}^t is the best previous position along the d-th dimension of the i-th particle in the t-th iteration; g_d^t is the best previous position among all the particles along the d-th dimension in the t-th iteration. From (44) and (45), we can know that all the particles follow the best solution obtained in the search process, which will lead the particles converge to a certain position and lose the diversity of population quickly. The improved PSO (IPSO) should satisfy the following requirements for enhancing the comprehensive performance of the basic PSO.

(1) The IPSO should have strong abilities both in terms of global searching and local searching.

(2) The IPSO should not introduce too many extra hyperparameters needed to be set.

(3) The IPSO should be intuitive enough and easy to adjust.

(4) The IPSO should be suitable for solving different optimization problems.

As we all know that the excessively concentrated particle swarm is easy to be trapped in local optima due to the particles are similar to each other. So the basic PSO should be improved to avoid the excessive aggregation of particles without influencing the local convergence speed. According to the above analysis, we proposed an IPSO algorithm with a

penalty term (PTPSO) to achieve a trade-off between exploration and exploitation abilities in this paper. The designed penalty term can dynamically adjust the updating velocity of particles in terms of the aggregation degree of particle swarm. In order to introduce the definition of penalty term, the distance between the i-th particle and the position of the current optimal solution in the t-th iteration is expressed as follows:

$$d_i^t = \sqrt{\sum_{d=1}^{D} (x_{id}^t - g_{id}^t)^2}, \tag{46}$$

where d_i^t is the Euclidean distance between the i-th particle and the position of the current optimal solution in the t-th iteration. For measuring the gathering degree of particle swarm, the density of aggregation defined as (47) is proposed.

$$\rho^t = \frac{\sum_{i}^{M} 1\left\{d_i^t < \gamma d_{max}\right\}}{M}, \tag{47}$$

where ρ^t is the defined aggregation density of particle swarm; $0 < \gamma < 1$ is the proportionality factor; d_{max} is the maximum straight-line distance in the searching space depended on the optimization problem. γd_{max} denotes the distance threshold that can reflect whether the particles are congregating around the current optimal particle. In order not to affect the performance when the particle swarm searching normally, the value of penalty term needs to be smaller when ρ^t is less than a certain threshold and it needs to increase dramatically when ρ^t is greater than this threshold. The adaptive punish coefficient is defined as follows:

$$p_c = \frac{a^{\rho^t - \rho_c} - a^{-\rho_c}}{1 - a^{-\rho_c}}, \tag{48}$$

where p_c is the coefficient of penalty term; $a > 1$ is the factor used for adjusting the curve shape of p_c; ρ_c is the critical value of aggregation density. From (48) we can know that the value of p_c is equal to 0 when ρ^t is equal to 0, and the value of p_c is equal to 1 when ρ^t is equal to ρ_c. Fig. 9 shows the relationship between p_c and ρ^t when a and ρ_c take different values.

It can be seen form Fig. 9 that the penalty term can hardly change the motion of particles when the particles are relatively dispersive and the effects of penalty term on the updating velocity of particles are powerful when the particles are excessively aggregated. In addition, according to the definition of (47), a higher γ indicates that the threshold of gathering condition is more easily to be satisfied. Therefore, the value of penalty term should decrease with increasing γ. Based on the above analysis, the velocity and position updating rule of IPSO can be formulated as follows:

$$v_{id}^{t+1} = w \times v_{id}^t + c_1 r_1 \left(p_{id}^t - x_{id}^t\right) + c_2 r_2 \left(g_d^t - x_{id}^t\right) + \overbrace{p_c \frac{(1-\gamma) v_{max}}{\sqrt{D}}}^{penalty\ term} r_3, \tag{49}$$

$$x_{id}^{t+1} = x_{id}^t + v_{id}^{t+1}, \tag{50}$$

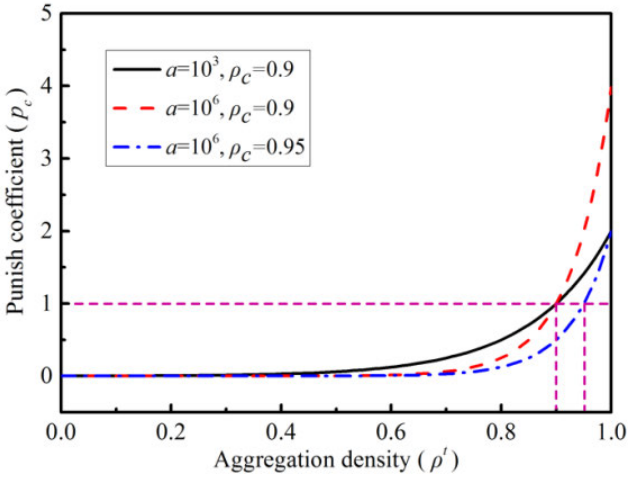

FIGURE 9. The relationship between the punish coefficient and aggregation density.

where r_3 is the independent random number uniformly distributed in the range of [0, 1]. We can learn form (49) that the proposed IPSO algorithm is sample in structure and can dynamically adjust the motion of each particle after the parameters γ, a and ρ_c are determined. The added hyper-parameters are well-defined, intuitive and easy to be set. In order to evaluate the proposed PTPSO algorithm, four non-linear benchmark functions are used here. The detailed information of the test problems are given in Table 2. In this section, the proposed strategy is compared with some PSO variants studied in the relevant literatures and Table 3 shows the summary of modified PSO algorithms analyzed in this paper.

For each minimization test problem shown in Table 2, x^* is the best solution to the test problem and $f(x^*)$ denotes the corresponding optimum fitness value for that function. Table 3 shows the differences between the PSO variants analyzed in this paper and the basic PSO and the relevant parameter values of each algorithm. In order to investigate the performance of the optimization algorithms, the strategies listed in Table 3 are used to search the optimal solutions of benchmark functions in the Table 2. For all the optimization algorithms mentioned above, the number of particles (M) is 50 and the number of iterations for each run (T) is 1000. Other parameters of the optimization algorithms are shown in Table 3. All the optimization algorithms are simulated on the same computer and software. The optimization results for each algorithm on each benchmark function are analyzed in this paper. Fig. 10 shows the means and the standard deviations of the benchmark function values found in 100 runs. Note that the calculation results of the proposed scheme in Fig. 10(d) are magnified 20 times for comparing the performance of different strategies more clearly. It can be seen form Fig. 10 that the optimized results of PTPSO algorithm (p_3) have smaller means and standard deviations than other PSO variants introduced in this paper, which indicates that the proposed strategy has more stable and powerful searching performance. By setting the parameters γ, a, and ρ_c properly,

TABLE 2. The benchmark functions employed for testing.

Name	Test function	Dimension	Search space	x^*	$f(x^*)$
Griewank	$\frac{1}{4000}\sum_{i=1}^{D} x_i^2 - \prod_{i=1}^{D} \cos\left(\sqrt{x_i}\right)+1$	50	$[-500, 500]^D$	$[0,\cdots,0]$	0
Rastrigin	$\sum_{i=1}^{D} (x_i^2-10\cos(2\pi x_i)+10)$	5	$[-20, 20]^D$	$[0,\cdots,0]$	0
Ackley	$-20\exp\left(-0.2\sqrt{\frac{1}{D}\sum_{i=1}^{D} x_i^2}\right) - \exp\left(\frac{1}{D}\sum_{i=1}^{D}\cos(2\pi x_i)\right)+20+e$	20	$[-30, 30]^D$	$[0,\cdots,0]$	0
Sphere	$\sum_{i=1}^{D} x_i^2$	30	$[-10, 10]^D$	$[0,\cdots,0]$	0

TABLE 3. Different PSO variants to be compared.

Label	Different strategies	Parameters setting	Reference
P_1	Basic PSO	w=0.9, c_1=c_2=2, v_{max}=2x_{max}	--
P_2	$v_{id}^{t+1}=k\left[v_{id}^t+c_1r_1\left(p_{id}^t-x_{id}^t\right)+c_2r_2\left(g_{id}^t-x_{id}^t\right)\right]$ $Where\ k=\frac{2}{\lvert 2-\varphi-\sqrt{\varphi^2-4\varphi}\rvert}$, $\varphi=c_1+c_2$, $\varphi>4$	φ=4.1, c_1=c_2=2.05 v_{max}=x_{max}	[32]
P_3	$v_{id}^{t+1}=wv_{id}^t+c_1r_1\left(p_{id}^t-x_{id}^t\right)+c_2r_2\left(g_{id}^t-x_{id}^t\right)+\frac{p_c r_3(1-\gamma)v_{max}}{\sqrt{D}}$ $Where\ p_c=\frac{a^{\rho^t-\rho_c}-a^{-\rho_c}}{1-a^{-\rho_c}}$	w=0.729, c_1=c_2=1.49445, a=10^6 ρ_c=0.99, γ=0.05, v_{max}=x_{max}	This paper
P_4	$w=w_{initial}u^{-iter}$	$w_{initial}$=0.9, c_1=c_2=2 u=1.001, v_{max}=2x_{max}	[33]
P_5	$w=\frac{iter_{max}-iter}{iter_{max}}(w_{max}-w_{min})+w_{min}$	w_{max}=0.9, w_{min}=0.4, c_1=c_2=2 v_{max}=2x_{max}	[34, 35]
P_6	$w_i^t=w_{initial}-\alpha\left(1-h_i^t\right)+\beta s$	$w_{initial}$=0.729, c_1=c_2=2 α=0.3, β=0.4, v_{max}=2x_{max}	[36]
P_7	$w=0.5+\frac{rand(\cdot)}{2}$	c_1=c_2=2, v_{max}=2x_{max}	[37]

the proposed PTPSO is suitable for solving different optimization problems. In this paper, the optimization algorithms are considered to have converged when the change of fitness value is less than 10^{-6}. The number of iterations when the algorithms achieve convergence is analyzed and Fig. 11 shows the means and the standard deviations of the iterations found in 100 runs.

Fig. 11 shows that the modified PSO algorithm p_2 has better convergence performance, which also is verified by [32]. However, the global searching ability of p_2 is not fully utilized and the fitness values found by p_2 have higher means and standard deviations. The proposed improved strategy is equivalent to add the designed penalty term on p_2, which can balance the local and global search capabilities and improve the comprehensive performance of optimization algorithm. Compared with p_2, the proposed scheme (p_3) needs more iterations to achieve convergence but can get better optimization results. During the course of the experiments, it was also found that the searching advantages of the proposed PTPSO become more obvious when the searching space and dimensions of test problems are greater. According to the analysis above, the proposed strategy has excellent performance and can be used for solving the mechanism optimization problem of designed master manipulator.

C. MECHANISM OPTIMIZATION RESULTS ANALYSIS

In this section, the dimensions of links are optimized based on the proposed optimization index by utilizing the PTPSO algorithm. Among all the linkage dimensions, a_4, a_5, d_2, d_5, and d_6 are limited by the structural requirements of the proposed master manipulator and have small variation range. In addition, we can know that the Jacobian matrix of the proposed mechanism has no connection with a_5, d_2, d_5, and d_6 from (33) and (34). So, a_1, a_3, and d_3 are optimized in this paper to improve the comprehensive performance of the designed master device. Other parameters can be initialized reasonably based on their range in the beginning of design. Table 4 shows the basic information of the fitness function and optimization algorithm. Based on the basic information shown in Table 4, the fitness function f was optimized by utilizing the proposed PTPSO algorithm to search the optimal linkage dimension. Then the optimized results were analyzed and the iterative process of f is shown in Fig. 12(a) and the iterative processes of f_k, f_l, and f_p are shown in Fig. 12(b).

From Fig. 12, we can know that the fitness value of f decreases with iterating and converges within 20 iterations. The kinematic performances, link utilization and motion precision are improved after optimizing. As shown in Fig. 12(a), $a_1 = 285.997$, $a_3 = 280.933$, and $d_3 = 130.030$ at the first

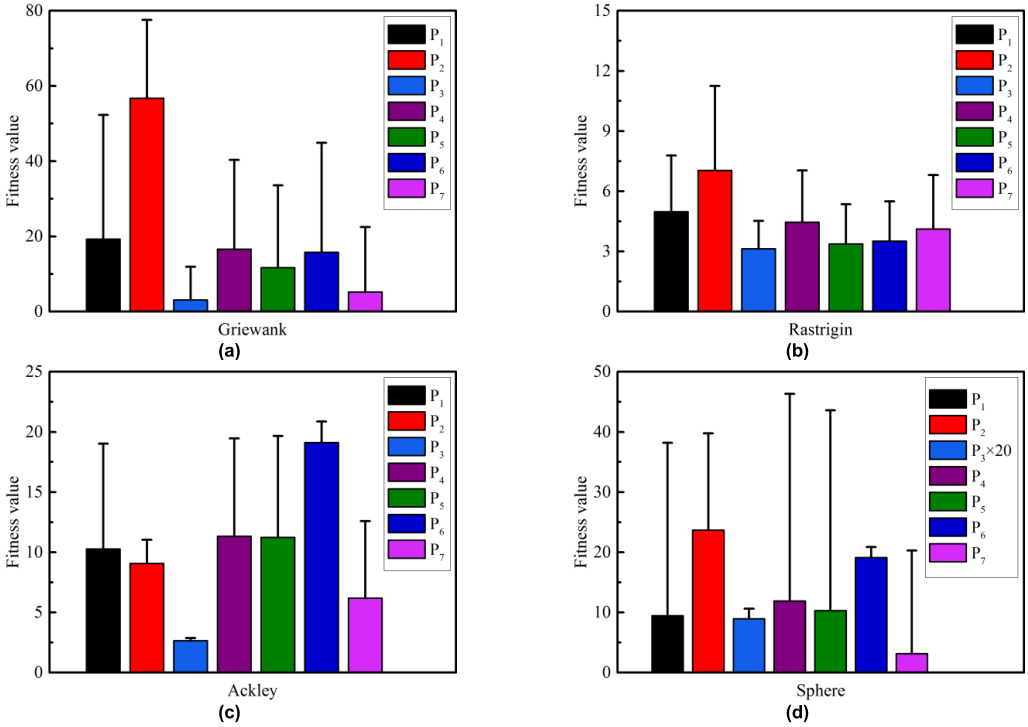

FIGURE 10. The means and the standard deviations of the benchmark function values found in 100 runs. (a) Griewank function. (b) Rastrigin function. (c) Ackley function. (d) Sphere function.

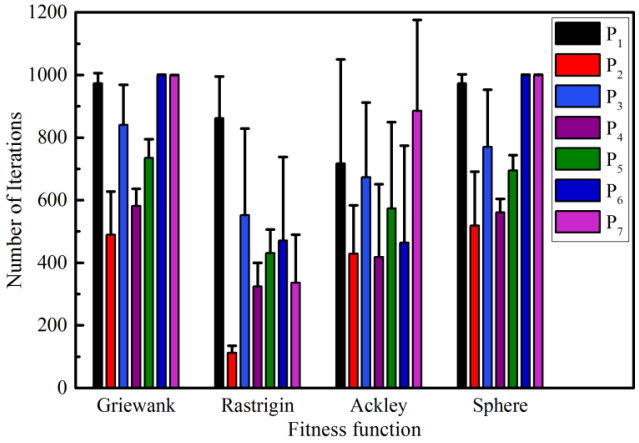

FIGURE 11. The means and the standard deviations of the iterations found in 100 runs.

iteration and $a_1 = 324.238$, $a_3 = 317.076$, and $d_3 = 50.000$ at the last iteration. In order to verify the effectiveness of the proposed strategy and evaluate the effects of optimization, the overall performances of mechanism at the initial and final iteration are compared. Since the distribution of conditional number in workspace can reflect the dexterity of mechanism and the reachable position lies on the lengths of links and the joint angles of position adjustment mechanism (q_1, q_2, and q_3), the reciprocals of conditional numbers ($1/k$) under different joint angles as shown in Fig. 13 are analyzed to evaluate the optimization results. In the each process of analysis, one certain joint angle is fixed and the optimization results of the initial and final iteration are compared.

The distribution maps shown in Fig. 13 point out that the reciprocals of conditional numbers at the initial iteration are lower than the reciprocals of conditional numbers at the final iteration, which indicates that the optimized mechanism has better isotropy and operability. Similar to the analysis above, the motion precision performances of mechanism at the initial and final iteration are studied in Fig. 14. Note that e_{max} shown in Fig. 14 denotes the maximum positioning under the influence of backlash. From Fig. 14, we can know that the manipulator has higher positioning error at the initial iteration, which verifies the optimization process can improve the kinematic accuracy of mechanism effectively. In order to evaluate the structure length utilization factor of mechanism with different link dimensions, the reachable workspace volumes at the initial and final iteration are compared. Fig. 15 shows the shape and volume of the reachable workspace and the sum of link lengths of these two mechanism settings, respectively.

From Fig. 15, we can know that the reachable workspace and the sum of link lengths are $1.6948 \times 10^8 \text{mm}^3$ and 696.960 mm respectively at the initial iteration and 1.9535×10^8 mm^3 and 691.314 mm respectively at the final iteration. That is, the optimized mechanism can achieve larger workspace with smaller link lengths and has higher utilization of structure length. Based on the above analysis, the dimension parameters of the proposed master manipulator can be determined. Among these parameters, a_1, a_3, and d_3 can be determined according to the optimization results, a_4, a_5, d_2, d_5, and d_6 can be determined by the structural constraints and the manual operation

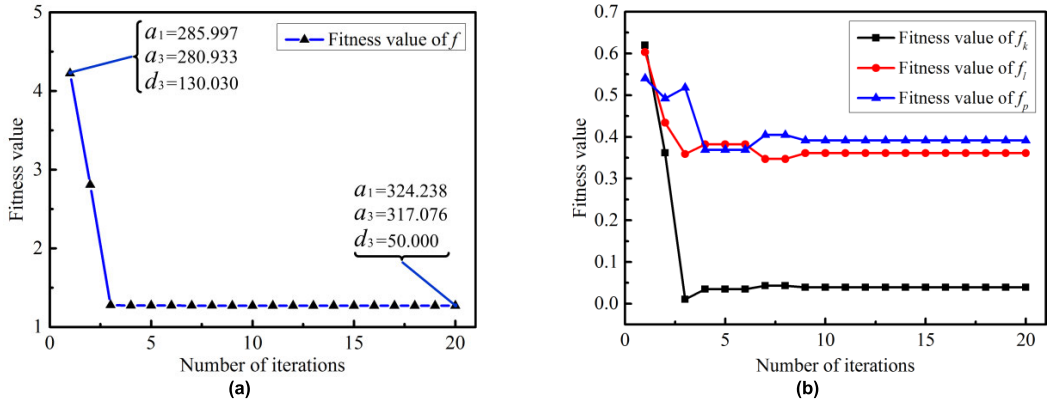

FIGURE 12. Change of the fitness values of f, f_k, f_l, and f_p. (a) Change of f. (b) Change of f_k, f_l, and f_p.

TABLE 4. The basic information of the problem to be optimized.

Parameter names	Parameters setting
Optimization algorithm	PTPSO
Fitness function	$f=4\frac{f_k-f_{kmin}}{f_{kmax}-f_{kmin}}+2\frac{f_l-f_{lmin}}{f_{lmax}-f_{lmin}}+\frac{f_p-f_{pmin}}{f_{pmax}-f_{pmin}}$
Dimension	3
Search space	$a_1\in[250, 350]$, $a_3\in[250, 350]$, $d_3\in[50, 150]$
Population of particles	10
Maximum iterations	20

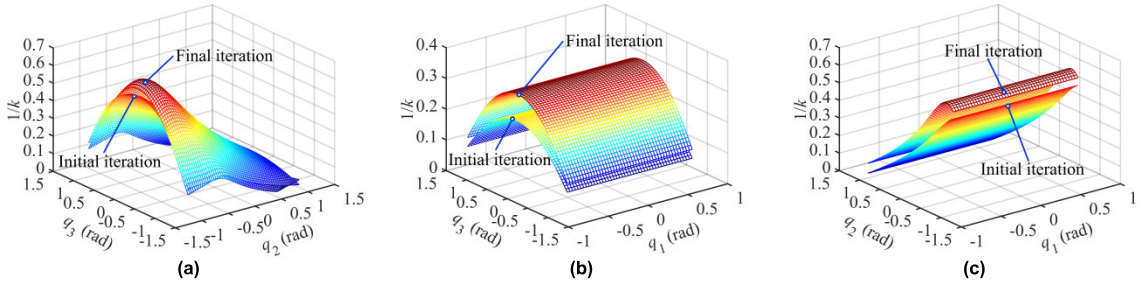

FIGURE 13. The distribution maps of the reciprocals of conditional numbers under different joint angles. (a) $q_1 = 0°$, $q_2 \in [-60°, 60°]$, $q_3 \in [-70°, 70°]$. (b) $q_2 = 0°$, $q_1 \in [-50°, 40°]$, $q_3 \in [-70°, 70°]$. (c) $q_3 = 0°$, $q_1 \in [-50°, 40°]$, $q_2 \in [-60°, 60°]$.

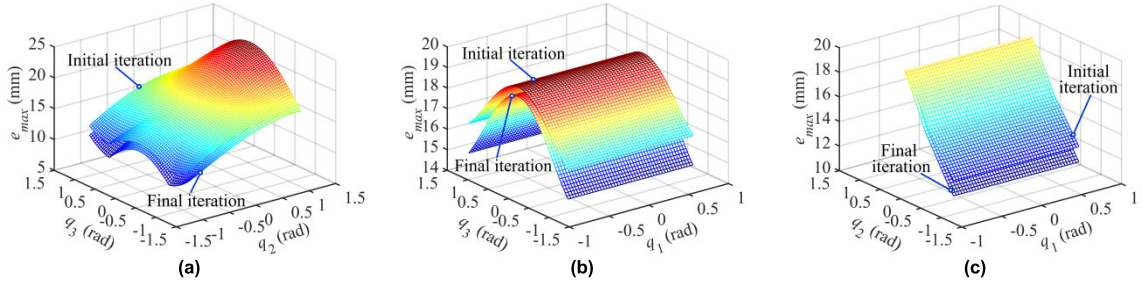

FIGURE 14. The maximum positioning error under the influence of backlash. (a) $q_1 = 0°$, $q_2 \in [-60°, 60°]$, $q_3 \in [-70°, 70°]$. (b) $q_2 = 0°$, $q_1 \in [-50°, 40°]$, $q_3 \in [-70°, 70°]$. (c) $q_3 = 0°$, $q_1 \in [-50°, 40°]$, $q_2 \in [-60°, 60°]$.

requirements of the master manipulator. According to the demands of processing, assembling, and actual operation, the value range of a_4, a_5, d_2, d_5, and d_6 are determined and shown in Table 5. Synthesizing Table 1, Table 5, and the optimization results, all D-H parameters of the designed manipulator are determined. Theoretic analysis and simulation results indicate that the comprehensive performances of the designed manipulator can be enhanced significantly by applying the proposed optimization index and the PTPSO algorithm.

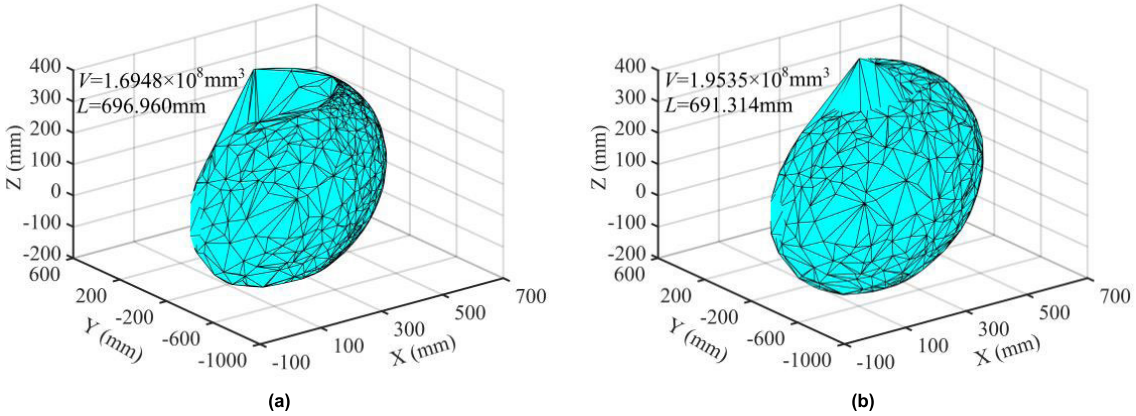

FIGURE 15. The shape and volume of the reachable workspace and the sum of link lengths at the initial and final iteration. (a) Initial iteration. (b) Final iteration.

TABLE 5. The value range of dimension parameters.

Parameters	a_4	a_5	d_2	d_5	d_6
Value range	[25, 50]	[160, 170]	[70, 80]	[60, 70]	[160, 170]

V. DISCUSSION

In this paper, a novel 9 DOFs master manipulator is designed and optimized for the applications of the laparoscopic surgical robots. For most of the traditional serial manipulators, the inherent mechanical characteristics can bring about coupled phenomenon between the position and posture of the holding point (as shown in Fig. 3), which may to a certain extent affect the comfort and intuition level of the surgeon's operation. Meanwhile, all the rotational joints of the proposed manipulator are active and the wire transmission and gear transmission are both employed for strengthening the output torque of the elbow pitch joint (as shown in Fig. 4 and Fig. 5). In the section III, the forward kinematics, inverse kinematics, and Jacobian matrix of the proposed manipulator are derived and analyzed. The results of kinematics analysis indicate that the position and posture of the holding point are mutually independent, which verifies the rationality and validity of the manipulator mechanism design. In order to study the performances of the designed master device comprehensively, an optimization index which considers the kinematic performances, motion precision, and structure length utilization of the mechanism is proposed in the section IV. An improved PSO with a penalty term is presented for enhancing the searching performances of the optimization algorithm. We also compared the proposed PTPSO algorithm with other PSO variants and Fig. 10 shows that the proposed PTPSO algorithm can obtain smaller means and standard deviations of the fitness functions. To finally verify the optimization performance of the proposed method, we take a_1, a_3, and d_3 as the optimized objective and Fig. 12 shows that the fitness value of the proposed optimization index decreases rapidly from the beginning and converges within 20 iterations. By extracting the link dimensions after the first and final optimization iteration (which is $a_1 = 285.997$, $a_3 = 280.933$, and $d_3 = 130.030$ and $a_1 = 324.238$, $a_3 = 317.076$, and $d_3 = 50.000$, respectively) as two different mechanism settings, several contrast experiments were also carried out for detailed comparison in terms of the dexterity, positional accuracy and structure length utilization of the mechanism (As shown in Fig. 13, Fig. 14, and Fig. 15, respectively).

In future research, we will analyze and optimize the proposed manipulator further. The missing parts of in this research will be studied. In addition, we will try to design a slave robot for the robot-assisted surgery systems and research the master-slave control algorithm.

VI. CONCLUSION

In this paper, a novel haptic master manipulator applied to the laparoscopic surgical robots is introduced along with its mechanism design and optimization method. The proposed master manipulator has larger workspace volume and better flexibility than parallel and serial-parallel hybrid mechanisms. To eliminate the coupled motion exists in the mechanism, the parallelogram mechanism and the position compensation mechanism are both adopted in the designed manipulator, through which the position and posture of the holding point can be decoupled completely. Wire transmission and gear reducer are both employed to avoid the extra volume and friction torque increment of the transmission mechanism. The derived kinematics solutions show that the proposed strategy could significantly reduce the computational complexities along the kinematics analysis. To better optimize the mechanical settings of the proposed manipulator, a mechanism optimization index that considers the global kinematic performances, global positioning

accuracy, and structure length utilization is proposed along with an improved PSO algorithm that contains a penalty term (PTPSO). Results of the comparative experiments between the PTPSO algorithm and other PSO variants have shown that the proposed strategy can balance the local and global search capabilities and improve the performance of the optimization algorithm synthetically. Finally, the dimensions of links are optimized based on the proposed optimization index by utilizing the PTPSO algorithm and additional contrast experiments have demonstrated that the kinematic performances, movement precision and structure length utilization of the mechanism are actually improved after applying the optimization method.

APPENDIX

According to (35), the condition number of the Jacobian matrix (k) can be calculated by using the maximum and minimum singular values of the Jacobian matrix. However, it is very difficult to solve the singular values of the Jacobian matrix by using the analytical method. In this paper, in order to derive the analytic expression of k and reduce the calculation, the condition number of the Jacobian matrix is calculated by the following expression.

$$k = \|J\| \cdot \left\|J^{-1}\right\|, \tag{51}$$

where $\|\cdot\|$ denotes any norm of its matrix argument. In this paper, the Frobenius norm is adopted to calculate k.

$$\|J\| = \sqrt{tr(J^T J)} \tag{52}$$

After combining (51) and (52), the condition number of the master manipulator can be expressed as:

$$\begin{aligned} k = {} & ((2a_3^4cq_3^2 + a_1^2a_3^2 + 2a_3^2a_4^2 + a_1^2d_3^2 - a_1^2a_3^2cq_2^2 \\ & + a_1^2a_4^2cq_2^2 - a_1^2d_3^2cq_2^2 + 2a_3^2d_3^2cq_3^2 + 4a_3^3a_4cq_3 \\ & - a_1^2a_4d_3s(2q_2) + 2a_1a_3^3cq_3sq_2 + 2a_1^2a_3^2cq_2^2cq_3^2 \\ & + 2a_1a_3^2a_4sq_2 + 2a_1^2a_3a_4cq_2^2cq_3 + 2a_1a_3^2d_3cq_2cq_3^2 \\ & - 2a_1^2a_3d_3cq_2cq_3sq_2)/(a_1^2a_3^2cq_3^2(a_4^2cq_2^2 - d_3^2cq_2^2 \\ & + d_3^2 + a_3^2cq_2^2cq_3^2 + 2a_3a_4cq_2^2cq_3 - 2a_4d_3cq_2sq_2 \\ & - 2a_3d_3cq_2cq_3sq_2)))^{1/2} \times (2a_3^2cq_3^2 + a_1^2 + a_3^2 \\ & + 2a_4^2 + 2d_3^2 + 2a_1a_4sq_2 + 4a_3a_4cq_3 + 2a_1d_3cq_2 \\ & + 2a_1a_3cq_3sq_2)^{1/2} \end{aligned} \tag{53}$$

REFERENCES

[1] Y. Liang, Z. Du, W. Wang, and L. Sun, "A novel position compensation scheme for cable-pulley mechanisms used in laparoscopic surgical robots," *Sensors*, vol. 17, no. 10, p. 2257, 2017.

[2] Y. Liang, Z. Du, W. Wang, Z. Yan, and L. Sun, "An improved scheme for eliminating the coupled motion of surgical instruments used in laparoscopic surgical robots," *Robot. Auton. Syst.*, vol. 112, pp. 49–59, Feb. 2019. doi: 10.1016/j.robot.2018.11.006.

[3] W. Wang, C. Du, W. Wang, and Z. Du, "A PSO-optimized fuzzy reinforcement learning method for making the minimally invasive surgical arm cleverer," *IEEE Access*, vol. 7, pp. 48655–48670, 2019. doi: 10.1109/ACCESS.2019.2910016.

[4] H. Song, Z. Du, W. Wang, and L. Sun, "Singularity analysis for the existing closed-form solutions of the hand-eye calibration," *IEEE Access*, vol. 6, pp. 75407–75421, 2018. doi: 10.1109/ACCESS.2018.2882183.

[5] J. H. Palep, "Robotic assisted minimally invasive surgery," *J. Minimal Access Surg.*, vol. 5, no. 1, p. 1, 2009.

[6] L. Yu, W. Wang, and F. Zhang, "External force sensing based on cable tension changes in minimally invasive surgical micromanipulators," *IEEE Access*, vol. 6, pp. 5362–5373, 2018. doi: 10.1109/ACCESS.2017.2788498.

[7] O. Meireles and S. Horgan, "Applications of surgical robotics in general surgery," in *Surgical Robotics*. New York, NY, USA: Springer, 2011, pp. 743–761.

[8] C. Freschi, V. Ferrari, F. Melfi, M. Ferrari, F. Mosca, and A. Cuschieri, "Technical review of the da Vinci surgical telemanipulator," *Int. J. Med. Robot. Comput. Assist. Surg.*, vol. 9, no. 4, pp. 396–406, 2013.

[9] G. H. Ballantyne and F. Moll, "The da Vinci telerobotic surgical system: The virtual operative field and telepresence surgery," *Surg. Clin. North Amer.*, vol. 83, no. 6, pp. 1293–1304, 2003.

[10] S. J. Kenneth, A. J. Madhani, G. S. Guthart, G. D. Niemeyer, E. F. Duval, and S. J. J. Kenneth, "Master having redundant degrees of freedom," U.S. Patent 6 714 839 B2, Mar. 30, 2004.

[11] A. Bhardwaj, A. Jain, and V. Agarwal, "Preoperative planning simulator with haptic feedback for Raven-II surgical robotics platform,"in *Proc. 3rd Int. Conf. Comput. Sustain. Global Develop. (INDIACom)*, Mar. 2016, pp. 2443–2448.

[12] B. Hannaford, J. Rosen, D. W. Friedman, H. King, P. Roan, L. Cheng, D. Glozman, J. Ma, S. N. Kosari, and L. White, "Raven-II: An open platform for surgical robotics research," *IEEE Trans. Biomed. Eng.*, vol. 60, no. 4, pp. 954–959, Apr. 2013.

[13] R. Konietschke, U. Hagn, M. Nickl, S. Jorg, A. Tobergte, G. Passig, U. Seibold, L. Le-Tien, B. Kubler, M. Groger, F. Frohlich, C. Rink, A. Albu-Schaffer, M. Grebenstein, T. Ortmaier, and G. Hirzinger, "The DLR MiroSurge—A robotic system for surgery," in *Proc. IEEE Int. Conf. Robot. Automat.*, May 2009, pp. 1589–1590.

[14] U. Hagn, R. Konietschke, A. Tobergte, M. Nickl, S. Jörg, B. Kübler, G. Passig, M. Gröger, F. Fröhlich, U. Seibold, L. Le-Tien, A. Albu-Schäffer, A. Nothhelfer, F. Hacker, M. Grebenstein, and G. Hirzinger, "DLR MiroSurge: A versatile system for research in endoscopic telesurgery," *Int. J. Comput. Assist. Radiol. Surg.*, vol. 5, no. 2, pp. 183–193, Mar. 2010.

[15] A. Tobergte and P. Helmer, "A disturbance observer for the sigma.7 haptic device," in *Proc. IEEE/RSJ Int. Conf. Intell. Robots Syst.*, Nov. 2013, pp. 4964–4969.

[16] A. Tobergte, P. Helmer, U. Hagn, P. Rouiller, S. Thielmann, S. Grange, A. Albu-Schäffer, F. Conti, and G. Hirzinger, "The sigma.7 haptic interface for MiroSurge: A new bi-manual surgical console," in *Proc. IEEE/RSJ Int. Conf. Intell. Robots Syst.*, Sep. 2011, pp. 3023–3030.

[17] D. Stephan, H. Sälzer, and F. Willeke, "First experiences with the new senhance Telerobotic system in visceral surgery," *Visceral Med.*, vol. 34, no. 1, pp. 31–36, 2018.

[18] S. G. Alletti, C. Rossitto, S. Cianci, E. Perrone, S. Pizzacalla, G. Monterossi, G. Vizzielli, S. Gidaro, and G. Scambia, "The Senhance surgical robotic system ('Senhance') for total hysterectomy in obese patients: A pilot study," *J. Robotic Surg.*, vol. 12, no. 2, pp. 229–234, 2018.

[19] J. H. Lim, W. J. Lee, D. W. Park, H. J. Yea, S. H. Kim, and C. M. Kang, "Robotic cholecystectomy using Revo-i Model MSR-5000, the newly developed Korean robotic surgical system: A preclinical study," *Surgical Endoscopy*, vol. 31, no. 8, pp. 3391–3397, 2017.

[20] K. D. Chang, A. A. Raheem, Y. D. Choi, B. H. Chung, and K. H. Rha, "Retzius-sparing robot-assisted radical prostatectomy using the Revo-i robotic surgical system: Surgical technique and results of the first human trial," *BJU Int.*, vol. 122, no. 3, pp. 441–448, 2018.

[21] H. Sang, S. Wang, J. Li, C. He, L. A. Zhang, and X. Wang, "Control design and implementation of a novel master-slave surgery robot system, MicroHand A," *Int. J. Med. Robot. Comput. Assist. Surg.*, vol. 7, no. 3, pp. 334–347, 2011.

[22] A. Talasaz, A. L. Trejos, S. Perreault, H. Bassan, and R. V. Patel, "A dual-arm 7-degrees-of-freedom haptics-enabled Teleoperation test bed for minimally invasive surgery," *J. Med. Devices*, vol. 8, no. 4, 2014, Art. no. 041004.

[23] Y. Li, Z. Yan, H. Wang, Z. Du, and Y. Zhang, "Design and optimization of a haptic manipulator using series-parallel mechanism," in *Proc. IEEE Int. Conf. Mechatronics Automat.*, Aug. 2012 pp. 2140–2145.

[24] P. Wisanuvej, G. Gras, K. Leibrandt, P. Giataganas, C. A. Seneci, J. Liu, and G.-Z. Yang, "Master manipulator designed for highly articulated robotic instruments in single access surgery," in *Proc. IEEE/RSJ Int. Conf. Intell. Robots Syst. (IROS)*, Sep. 2017, pp. 209–214.

[25] H. Takahashi, T. Yonemura, N. Sugita, M. Mitsuishi, S. Sora, A. Morita, and R. Mochizuki, "Master manipulator with higher operability designed for micro neuro surgical system," in *Proc. IEEE Int. Conf. Robot. Automat.*, May 2008, pp. 3902–3907.
[26] T. Wang, B. Pan, Z. Tang, Y. Fu, X. Niu, and S. Wang, "Design and analysis of a force reflection master manipulator for minimally invasive surgical robot," in *Proc. IEEE Int. Conf. Robot. Biomimetics (ROBIO)*, Dec. 2014, pp. 58–63.
[27] R. Ma, W. Wang, Z. Du, and G. Li, "Design and optimization of manipulator for laparoscopic minimally invasive surgical robotic system," in *Proc. IEEE Int. Conf. Mechatronics Automat.*, Aug. 2012, pp. 598–603.
[28] J.-W. Zhang and W. Xiong, "An improved particle swarm optimization algorithm and its application for solving traveling salesman problem," in *Proc. WRI World Congr. Comput. Sci. Inf. Eng.*, vol. 4, Mar./Apr. 2009, pp. 612–616.
[29] S. Dheeban, V. Deepak, L. Dhamodharan, and S. Elias, "Improved personalized e-course composition approach using modified particle swarm optimization with inertia-coefficient," *Int. J. Comput. Appl.*, vol. 1, no. 6, pp. 102–107, 2010.
[30] J. C. Bansal and K. Deep, "A modified binary particle swarm optimization for knapsack problems," *Appl. Math. Comput.*, vol. 218, no. 22, pp. 11042–11061, Jul. 2012.
[31] C. Gosselin and J. Angeles, "A global performance index for the kinematic optimization of robotic manipulators," *J. Mech. Des.*, vol. 113, no. 3, pp. 220–226, 1991.
[32] R. C. Eberhart and Y. Shi, "Comparing inertia weights and constriction factors in particle swarm optimization," in *Proc. Congr. Evol. Comput.*, vol. 1, Jul. 2000, pp. 84–88.
[33] B. Jiao, Z. Lian, and X. Gu, "A dynamic inertia weight particle swarm optimization algorithm," *Chaos Solitons Fractals*, vol. 37, no. 3, pp. 698–705, Aug. 2008.
[34] Y. Shi and R. C. Eberhart, "Empirical study of particle swarm optimization," in *Proc. Congr. Evol. Comput.-CEC99*, vol. 3, Jul. 1999, pp. 1945–1950.
[35] M. A. Arasomwan and A. O. Adewumi, "On the performance of linear decreasing inertia weight particle swarm optimization for global optimization," *Sci. World J.*, vol. 2013, pp. 1–12, Sep. 2013, Art. no. 860289.
[36] X. Yang, J. Yuan, J. Yuan, and H. Mao, "A modified particle swarm optimizer with dynamic adaptation," *Appl. Math. Comput.*, vol. 189, no. 2, pp. 1205–1213, 2007.
[37] R. C. Eberhart and Y. Shi, "Tracking and optimizing dynamic systems with particle swarms," in *Proc. Congr. Evol. Comput.*, vol. 1, May 2001, pp. 94–100.

YUNLEI LIANG was born in Heilongjiang, China, in 1991. He received the B.S. and M.S. degrees in mechatronics engineering from the Harbin Institute of Technology, Harbin, China, in 2014 and 2016, respectively, where he is currently pursuing the Ph.D. degree. His main research interests include the remote operating system of the minimally invasive surgical robot (MIS), surgery navigation, pHRI problems, and force/shape sensing problems and its applications in surgical robot.

LINING SUN received the B.S., M.S., and Ph.D. degrees from the School of Mechatronics Engineering, Harbin Institute of Technology, in 1985, 1988, and 1993, respectively, where he has been a Professor with the State Key Laboratory for Robotics and System, since 1999. His research interests include parallel robot, surgical robot, industrial robot, and micro robot.

ZHIJIANG DU received the B.S., M.S., and Ph.D. degrees from the School of Mechatronics Engineering, Harbin Institute of Technology, in 1995, 1997, and 2001, respectively, where he has been a Professor with the State Key Laboratory for Robotics and System, since 2006. He is currently the Deputy Director of the Robotics Institute of Harbin Institute of Technology. His research interests include surgical robot, industrial robot, and robot for special environment.

ZHIYUAN YAN is currently with the State Key Laboratory of Robotics and System, Harbin Institute of Technology. He has published over 15 articles, 14 of which have been included in SCI or EI. His research expertise is in the general areas of robotics and mechatronics. His research interests include master-slave control systems of minimally invasive surgical robot (MIS), augmented reality technology, and human–machine interaction technology. Dr. Yan is PI or Co-PI on ten proposals.

WEIDONG WANG received the B.S., M.S., and Ph.D. degrees in mechatronics engineering from the Harbin Institute of Technology, in 2002, 2004, and 2009, respectively, where he is currently with the State Key Laboratory of Robotics and System. His research expertise is in the general areas of robotics and mechatronics. His research interests include motion planning, computer vision, and human–machine interaction, and its application in field robot and surgery robot.